# Indexing brain state-dependent pupil dynamics with simultaneous fMRI and optical fiber calcium recording

Patricia Pais-Roldán[a,b,c], Kengo Takahashi[a,b], Filip Sobczak[a,b], Yi Chen[a,b], Xiaoning Zhao[a], Hang Zeng[a,b], Yuanyuan Jiang[a,d], and Xin Yu[a,d,1]

[a]High-Field Magnetic Resonance Department, Max Planck Institute for Biological Cybernetics, 72076 Tuebingen, Germany; [b]Graduate Training Centre of Neuroscience, International Max Planck Research School, University of Tuebingen, 72074 Tuebingen, Germany; [c]Medical Imaging Physics, Institute of Neuroscience and Medicine, Forschungszentrum Juelich, 52425 Juelich, Germany; and [d]Athinoula A. Martinos Center for Biomedical Imaging, Massachusetts General Hospital, Harvard Medical School, Charlestown, MA 02129

Edited by Marcus E. Raichle, Washington University in St. Louis, St. Louis, MO, and approved February 7, 2020 (received for review June 10, 2019)

**Pupillometry, a noninvasive measure of arousal, complements human functional MRI (fMRI) to detect periods of variable cognitive processing and identify networks that relate to particular attentional states. Even under anesthesia, pupil dynamics correlate with brain-state fluctuations, and extended dilations mark the transition to more arousable states. However, cross-scale neuronal activation patterns are seldom linked to brain state-dependent pupil dynamics. Here, we complemented resting-state fMRI in rats with cortical calcium recording (GCaMP-mediated) and pupillometry to tackle the linkage between brain-state changes and neural dynamics across different scales. This multimodal platform allowed us to identify a global brain network that covaried with pupil size, which served to generate an index indicative of the brain-state fluctuation during anesthesia. Besides, a specific correlation pattern was detected in the brainstem, at a location consistent with noradrenergic cell group 5 (A5), which appeared to be dependent on the coupling between different frequencies of cortical activity, possibly further indicating particular brain-state dynamics. The multimodal fMRI combining concurrent calcium recordings and pupillometry enables tracking brain state-dependent pupil dynamics and identifying unique cross-scale neuronal dynamic patterns under anesthesia.**

brain state | rat | anesthesia | multimodal imaging

Neural activity fluctuates at low frequencies (<0.1 Hz) to mediate arousal or attentional states during rest (1, 2). Studying such resting-state (rs) fluctuations at different scales makes it possible to identify the neuromodulatory schemes underlying the spontaneous transitions between different brain states (3–7). Functional MRI performed during rest (rs-fMRI) can be used to extract the temporal dynamics from different neuronal populations across the brain (8–10). The temporal correlation between remote areas can be used to map baseline functional connectivity patterns that portray so-called resting-state networks, which have been associated with particular neuropsychological states and have a potential prognostic value in clinical disorders (11–13). Alternatively, transitions between distinct brain states (e.g., sleep or attention) can be tracked as direct changes in the global fMRI signal, which has also been well-reported in animal brains under general anesthesia with rs-fMRI (4, 14–22). Several human and nonhuman primate studies have demonstrated that the global fMRI signal accurately reflects the momentary level of attention or arousal (1, 23, 24), suggesting a critical role of the ubiquitous spontaneous oscillations in orchestrating the transition between brain states. Additionally, human experiments where pupillometry was added to the fMRI measurement have identified some potential neural correlates of arousal (25–27), yet the mechanisms underlying spontaneous transitions toward varying brain states remain only partially understood.

Recently, experiments performed in rats have revealed key global signatures that precede brain-state changes during anesthesia by measuring the fMRI signal in parallel to the calcium-dependent neuronal and astrocytic activity (4), which indicates the potential of multimodal fMRI platforms to be applied in behaving rodents to track different brain states. However, despite ongoing efforts to set up an awake rodent multimodal fMRI platform (28–30), the potential stress and motion-related artifacts (31, 32), summed to the lack of a robust behavioral arousal measurement inside the MRI scanner, have prevented multimodal fMRI investigations of the brain state in awake rodents. Eye blinks, unconscious eye movements, and pupil-size variations can report the level of arousal (1) and condition of task performance (7, 33, 34) and reflect the level of cognitive processing (35), attention (36), fear (37), or reward anticipation (38). Animal experiments performed at the bench (e.g., electrophysiological studies) have allowed accurately testing the relationship between pupil dilations and neural activity specific to particular brain areas. Pupil fluctuations have been repeatedly linked to the activity of neurons in the noradrenergic locus coeruleus (LC) (39, 40) and mark cortical state changes (33, 34, 41–44), which places the pupil as an affordable arousal indicator to merge with other brain imaging schemes. These studies have linked pupil dilations to desynchronized cortical activity and depolarized states during walking-related arousal (33, 34, 41).

## Significance

**Resting-state fMRI (rs-fMRI) performed in animals allows investigating the spatial correlation patterns of brain function, which presents diverse oscillatory features in varied brain states, even under anesthesia. However, the link between global fMRI signal oscillations and fluctuations in the level of arousal, which can be indexed by spontaneous pupil dilations, is seldom investigated in rodent brains. Here, we established pupillometry with rs-fMRI and concurrent cortical calcium recordings in anesthetized rats, enabling brain-state fluctuation analysis across multiple scales. A unique positive correlation with pupil dilations was detected near noradrenergic cell group 5 (A5) in the ventral brainstem, which was associated with a specific coupling between spectrally different calcium waves, highlighting unique brain-state dynamics.**

Author contributions: P.P.-R. and X.Y. designed research; P.P.-R., K.T., Y.C., and Y.J. performed research; Y.C. and Y.J. provided technical support; P.P.-R., K.T., F.S., Y.C., X.Z., and H.Z. analyzed data; and P.P.-R. and X.Y. wrote the paper.

The authors declare no competing interest.

This article is a PNAS Direct Submission.



Data deposition: All fMRI datasets, as well as the synchronized calcium recordings and pupil-size vectors, reported in this paper have been deposited in Zenodo at https://doi.org/10.5281/zenodo.3677525.

[1]To whom correspondence may be addressed. Email: xyu9@mgh.harvard.edu.

This article contains supporting information online at https://www.pnas.org/lookup/suppl/doi:10.1073/pnas.1909937117/-/DCSupplemental.

First published March 5, 2020.

Pupillometry can be especially informative during anesthesia, where motor-driven behavioral measurements are not accessible to the experimenter. Kum et al. (43) showed that anesthetic washout (i.e., emergence from anesthesia) is accompanied by burst activity and mydriasis in rats, suggesting that lighter unconscious states during anesthesia could be tracked by measuring the pupil size.

Despite existing rodent studies combining electrophysiological measurements with pupillometry, to date there are no studies merging pupil dynamics with the activity of neuronal populations and concurrent whole-brain fMRI in rats. The goal of this work was to merge the bench measures with fMRI to create a platform that allows investigating the link between spatiotemporal changes in brain activity and transitory brain states that can be tracked with pupillometry. Here, GCaMP-mediated calcium signal changes were recorded from cortical neurons in parallel to whole-brain fMRI in anesthetized rats (4, 21) subjected to concurrent pupillometry. Based on the rs-fMRI signal and its correlation with pupil dilations, we identified the presence of oscillatory brain states under anesthesia, which were specifically represented by neuronal calcium dynamics. Besides tackling the technical challenge of performing pupillometry in small-animal MR scanners, we demonstrate the potential of this platform to investigate the mechanisms underlying brain-state transitions across multiple scales.

## Results

**Concurrent fMRI and Neuronal Calcium and Pupil Dynamics Track Brain-State Changes in the Anesthetized Rat.** We used a small MRI-compatible camera to track pupil dynamics from the rat eye in parallel to fMRI and obtain a measure of the brain-state fluctuation during anesthesia (*SI Appendix*, Fig. S1). The measure of pupil-size changes was introduced in a multiscale analysis workflow as illustrated in Fig. 1. Three main recordings were obtained in parallel: 1) video recording of the pupil, 2) optical fiber calcium recording (in the cingulate cortex, as well as in the barrel cortex in some rats), and 3) whole-brain fMRI imaging. First, the vector representing the pupil-size fluctuation was generated from the acquired video (45) (Fig. 2, *Top* trace, *SI Appendix*, Fig. S2, and Movie S1) (see *SI Appendix*, *Methods* for details). This vector of pupil dynamics was correlated with each fMRI voxel time course to obtain a pupil–fMRI correlation map (Fig. 3*A*). In addition, another correlation map was created by comparing the fMRI time courses with the first derivative of the pupil size (1d-pupil; i.e., pupil dilations) (Fig. 3*B*). Second, the pupil dilation–fMRI correlation map, considered a pupil-relevant spatial template, was spatially correlated with the original 4-dimensional fMRI (45) (i.e., a time-varying volume) to create a specific spatiotemporal correlation time course that provided an fMRI index of the brain state (Fig. 4*A* and Movie S2), similar to what has been shown in previous rs-fMRI arousal studies on nonhuman primates (1). Third, the pupil dynamics were studied in relation to the calcium signal fluctuation from the cortex (45), in particular the 2- to 3-Hz activity band, which showed the strongest power throughout the calcium spectrum (Figs. 2, *Bottom*, and 5*C* and *SI Appendix*, Fig. S3, *Lower Right*) (the spectral analysis of the calcium signals is explained in *SI Appendix*, *Methods*). Finally, the time course of the fMRI-inferred brain-state index was compared with the calcium dynamics from the cingulate cortex (Fig. 4 *D* and *E*). *SI Appendix*, Fig. S3 shows a summary pipeline with the main steps followed in this work. The relationship between the fMRI signals and the fMRI-inferred brain-state time course, as well as the pupil and calcium dynamics, is exemplified in Movie S2. Fig. 2 shows the brain-state fluctuation detected with the multimodal platform in a representative animal under anesthesia (another example is shown in *SI Appendix*, Fig. S4). Alternation between brain states was evidenced by the transition from constricted to dilated pupil or vice versa, which showed a strong correlation with the whole-brain fMRI signal fluctuation and with the neuronal calcium signal oscillation. It is noteworthy that the brain-state dynamics varied across different trials. This dynamicity can be presented by the index of pupillary unrest (PUI), which measures the variability in pupil size per run (*SI Appendix*, *Methods*) (46). The PUI was positively correlated with the SD of the pupil size, showing 43% of the total trials ($n = 71$ of 10 rats) with a PUI above 1,000, denoting salient low-frequency oscillatory patterns (*SI Appendix*, Fig. S5). Together, the acquired measures indicate that the multimodal platform merging fMRI, pupillometry, and calcium imaging enables a cross-scale investigation of the varying brain states in anesthetized animals.

**Correlation Analysis of Whole-Brain fMRI with Pupil Dynamics in Anesthetized Rats.** Simultaneous fMRI and pupillometry allowed us to compute 2 pupil-correlated fMRI maps in the anesthetized

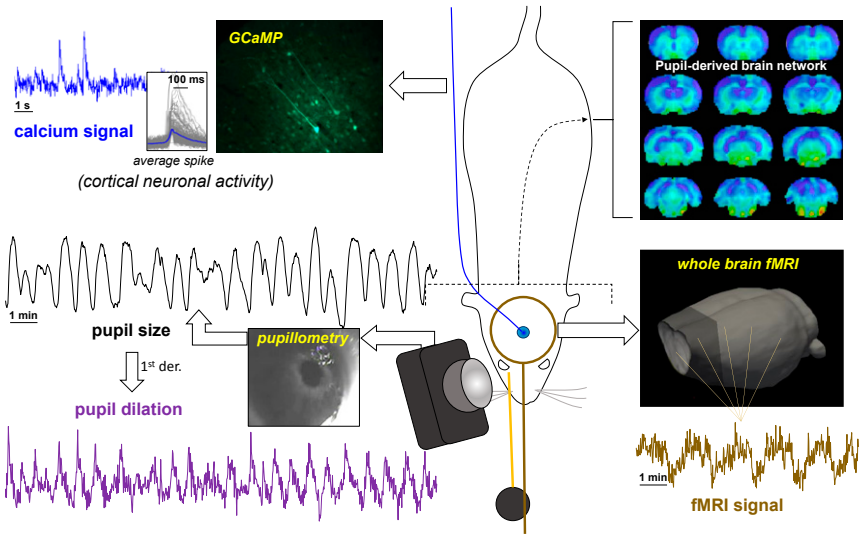


**Fig. 1.** Multimodal GCaMP–pupil–fMRI platform. The scheme shows the setup used to acquire concurrent neuronal calcium signals from the cingulate cortex (GCaMP-based), pupillometry, and whole-brain fMRI, which allows building a pupil–fMRI correlation map ("pupil-derived brain network"), and study the relationship between whole-brain patterns, neurophysiological features, and arousal states.

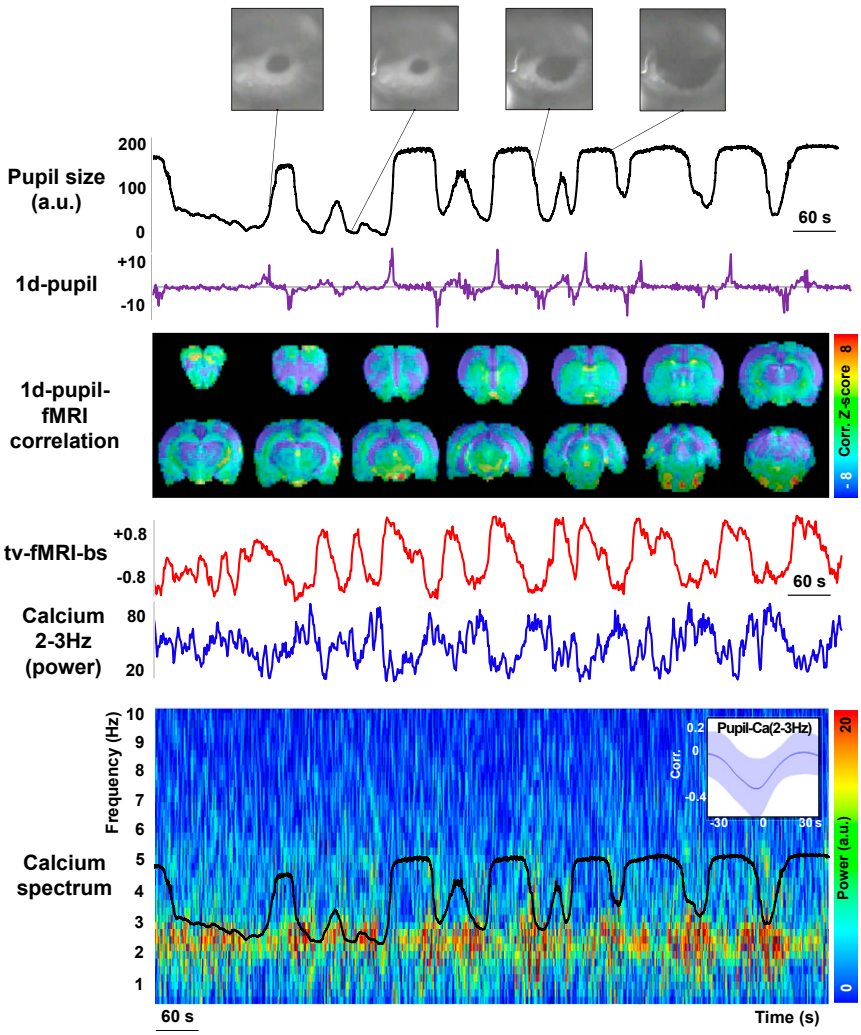


**Fig. 2.** Tracking brain-state changes with pupillometry, fMRI, and calcium imaging. The traces, map, and spectrum show an example of the measures obtained concurrently during a 15-min scan in an anesthetized rat. Note the negative correlation between 2-3-Ca and the tv-fMRI-bs, and between 2-3-Ca and the pupil diameter. The *Inset* over the power spectrum decomposition of the calcium signal (*Bottom*) shows an averaged cross-correlation between pupil-size changes and 2-3-Ca ±SD across trials. a.u., arbitrary units.

state. The map in Fig. 3*A* shows the voxel-wise correlation between the pupil-size time course and the fMRI signals, indicating a negative correlation in most of the cerebral cortex, thalamus, septal nuclei, and superior colliculus, some of which have been previously identified as neural correlates of pupil dilations during wakefulness [i.e., cingulate cortex or superior colliculus (47, 48)]. While the pupil size correlates with the arousal level during wakefulness (26, 40), specific brain regions relevant to the switch between arousal states can be potentially assessed by correlating the fMRI signal with the first-order derivative of the pupil-size dynamic time course (26, 38, 49); therefore, we also performed correlation analysis between blood oxygen level-dependent (BOLD) fMRI and 1d-pupil (e.g., the purple trace in Fig. 2). The resulting 1d-pupil-fMRI map showed that the areas exhibiting negative correlation with the pupil size were also negatively correlated with 1d-pupil and, in addition to it, an area in the brainstem was found positively correlated with the 1d-pupil time course, which was not detected in the pupil-size correlation map (Fig. 3). The positively correlated brainstem overlapped with the rostral A5 area (Fig. 3 *C* and *D*), which contains primarily noradrenergic cells and projects to the major subcortical arousal nuclei through the reticular formation pathway (50). It is worth noting that no significant positive correlation was observed in other subcortical nuclei involved in arousal regulation, for example the LC (39) or the central and mediodorsal thalamic nuclei (4, 51).

To study the temporal relationship between the fMRI and the pupil dynamics, the whole-brain fMRI time courses were also correlated with a lagged version of the pupil size or 1d-pupil. This analysis resulted in 2 sets of maps (*SI Appendix*, Fig. S6*A*), which indicated that the areas correlating negatively with the pupil size did so at short lags (i.e., faster hemodynamic response functions [HRFs]), with longer lags reducing their correlation value, while the same areas were well-correlated with 1d-pupil at all lags. Importantly, the positive correlation in the brainstem, only present in the 1d-pupil correlation map, was mainly observed at short lags (using fast HRFs). In order to investigate the temporal dynamics of the positively correlated area in the brainstem with respect to the negative global signal in the context of brain-state regulation, we averaged the fMRI time courses from both functional clusters and performed cross-correlation analysis with respect to the pupil size or to 1d-pupil. The positive cluster (brainstem) was most correlated with 1d-pupil at a 0-s lag (pink wave in *SI Appendix*, Fig. S6*B*; first derivative). In contrast, the negative cluster exhibited its maximum correlation 5 s later, in agreement with the voxel-wise correlation results. The results of this analysis indicated that the brainstem activates during pupil

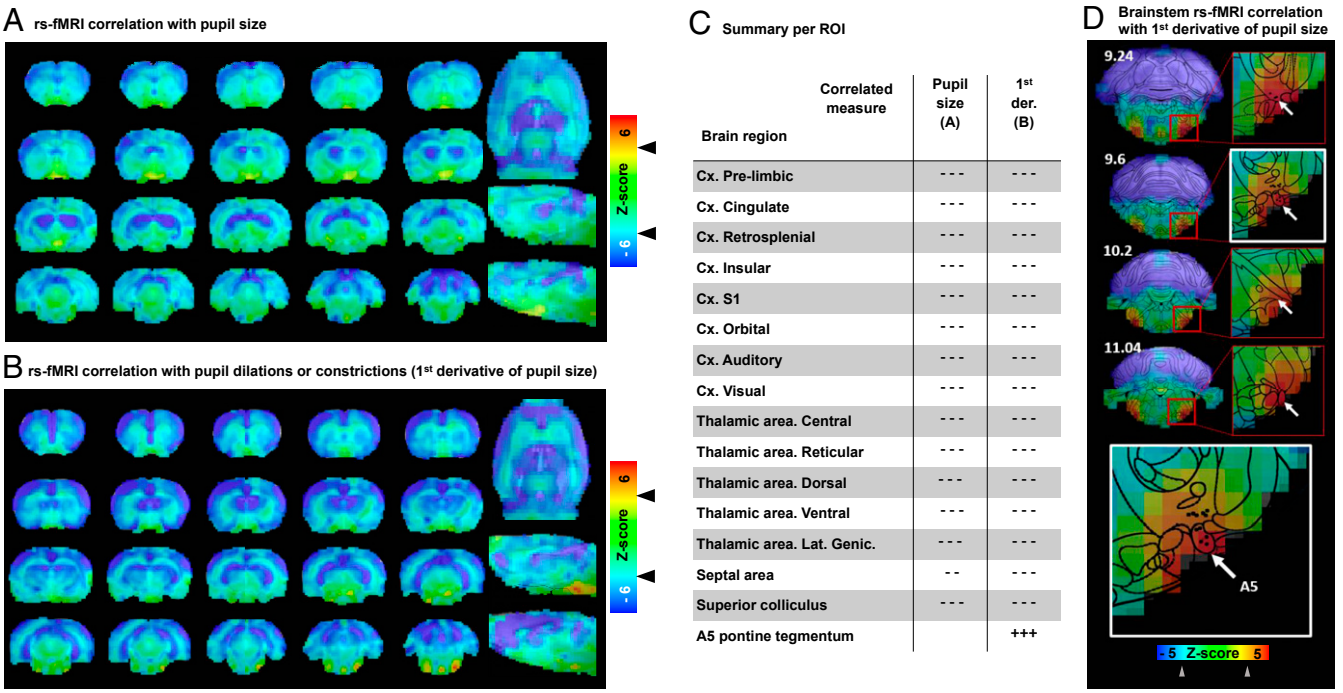


**Fig. 3.** Covariability of the fMRI signals with pupil dynamics. (*A* and *B*) Statistic maps of the fMRI correlation with pupil size (*A*) or the first derivative of the pupil size (*B*); $n = 71$ trials from 10 animals. The black arrowheads in the color bars identify a $P$ value of $\pm 0.01$. (*C*) Region-specific correlation analysis for each of the 2 conditions (*A* and *B*). [– – –]/[+ + +], $P < 0.001$; [– –], $P < 0.005$. (*D*) Statistic first derivative–fMRI correlation map focused on the brainstem region to show the positive correlation detected in an area matching noradrenergic group A5 [white arrows, based on a rat brain atlas (82)]. Arrowheads in the color bar identify a $P$ value of $\pm 0.01$.

dilation but not necessarily after the pupil has increased its size, which coincides with the globally reduced BOLD fMRI signal that cofluctuates with pupil-size changes. To represent a brain state more timely correlated with pupil dynamics, we are using the 1d-pupil–fMRI correlation map as a template in the successive steps of our analysis.

**Pupil–fMRI–Derived Index to Measure the Brain State.** As shown in Fig. 4 and Movie S2, the momentary pupil-linked brain state can be inferred from each acquired rs-fMRI volume by calculating its spatial correlation with the 1d-pupil–fMRI correlation map. Concatenation of the spatial correlation values produces a vector of the time-varying fMRI-inferred brain state (tv-fMRI-bs) (1). To specify the neuronal correlates of the inferred brain-state fluctuation, the power profile of the 2- to 3-Hz calcium fluctuation (2-3-Ca) was cross-correlated with the tv-fMRI-bs and with the varying pupil size, showing strong correlation features with both signals (Fig. 4 *E* and *G*). The tv-fMRI-bs was positively correlated with the pupil dynamics (Fig. 4 *B* and *C*) but showed a negative correlation with the 2-3-Ca oscillation (Fig. 4 *D* and *E*; cross-validation is shown in *SI Appendix*, Fig. S7). In addition, the neuronal calcium recordings from cingulate and barrel cortex in our anesthetized rats covaried (negatively) with pupil-size changes, showing a decrease of the 2-3-Ca upon dilations (Fig. 4 *G* and *H* and *SI Appendix*, Fig. S8), consistent with the negative correlation observed from the same cortical region in the pupil–fMRI correlation map. The salient correlation features observed across multiple trials between the tv-fMRI-bs, the calcium oscillation from the cortex, and the pupil dynamics present a generalized 3-way interaction scheme to elucidate brain-state changes in anesthetized rats (Fig. 4*F*).

**Identification of Brain State-Dependent Pupil Dynamics under 2 Distinct Cortical States under Anesthesia.** The calcium signal recorded from the cortex exhibited 2 main components: a slowly fluctuating baseline (<0.5 Hz) and oscillations within the frequency range typical of the electroencephalogram (EEG) (strongest at 2 to 3 Hz, as shown in Figs. 2 and 5*C* and *SI Appendix*, Fig. S3). In particular, the 2- to 3-Hz calcium transients have been verified with simultaneous local field potential and multiunit activity recordings showing a strong correlation (Fig. 5 *B*, *E*, and *G*). Analysis of the neuronal activity at both frequency ranges provided an additional dynamic feature to depict the neurophysiological state of animals. A subset of trials showed strong cross-frequency coupling between the baseline and 2-3-Ca (Fig. 5*H*, red dots) (21); however, ~40% of the trials demonstrated poor correlation or uncoupled cross-frequency calcium dynamics (Fig. 5*H*, black dots), similar to the dissociation of phase and amplitude coupling observed in previous EEG studies (52, 53). The 1d-pupil–fMRI correlation maps acquired from both groups independently showed a negative correlation through most of the brain (Fig. 5*I*), similar to the correlation map acquired from all trials together (Fig. 3*B*). However, the positive correlation in the brainstem was significantly higher in the calcium-uncoupled group (Fig. 5*I*). Interestingly, the SD of the pupil was also higher in calcium-uncoupled trials (*SI Appendix*, Fig. S9*C*, dots outside the red box), indicating a brain state-dependent pupil dynamic behavior. In all, the assessment of cross-frequency coupling from the calcium data suggested the existence of distinct modes of brain-state dynamics under anesthesia, also supported by the opposite correlation between the calcium baseline and the tv-fMRI-bs in the 2 identified groups (*SI Appendix*, Fig. S9*D*), which is consistent with the EEG observed during brain-state switches under anesthesia (54, 55). Altogether, our data indicate that the cross-frequency coupling of the calcium signal constitutes a potential marker to further differentiate between periods of stronger or weaker pupil control during the dynamic brain state.

## Discussion

In this work, simultaneous whole-brain fMRI and optical fiber-mediated neuronal calcium recordings were acquired to specify brain state-dependent pupil dynamics in anesthetized rats. Cross-correlation

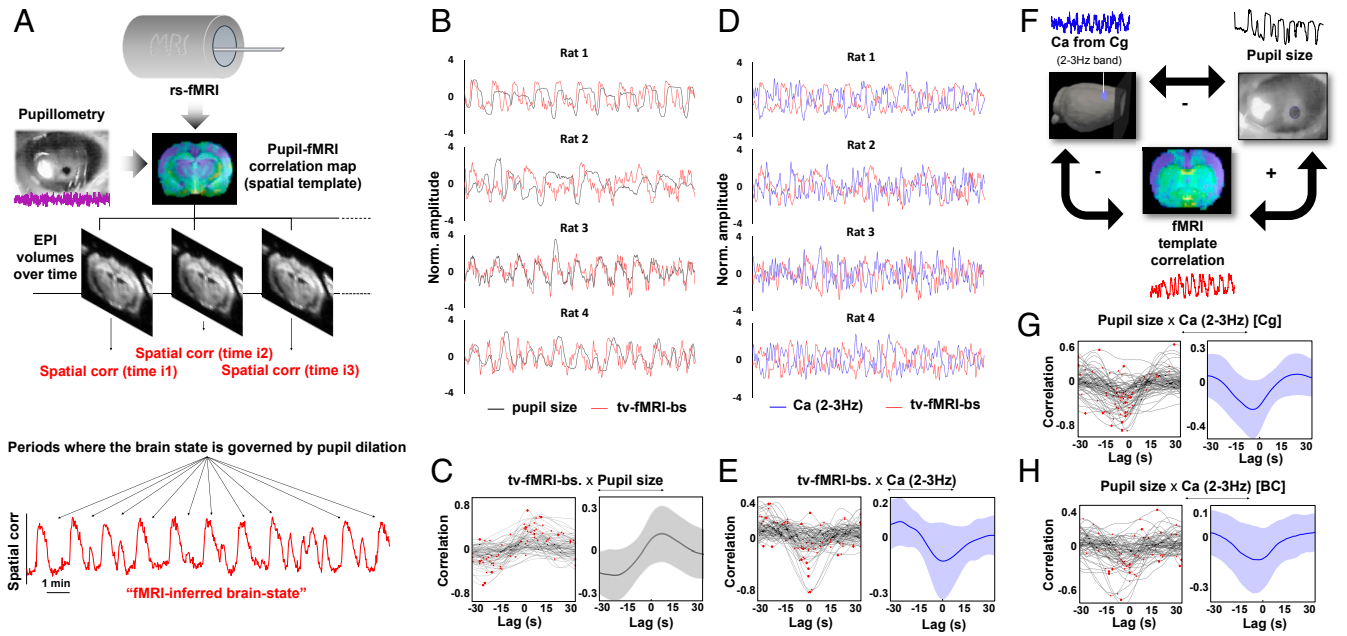


**Fig. 4.** Acquisition and properties of the pupil-governed brain-state time course. (*A*) Schematic showing how the time-varying fMRI-inferred brain-state (tv-fMRI-bs) time course was computed for each fMRI scan. (*B*) Four pairs of time courses from different animals are shown to exemplify the similarity between the fluctuations in the pupil size (black traces) and the fluctuations in the tv-fMRI-bs (red traces). (*C*) Cross-correlation between the pupil size and the tv-fMRI-bs. (*D*) Four pairs of time courses from different animals exemplify the inverse relationship between the tv-fMRI-bs (red traces) and the population activity at 2 to 3 Hz from the cingulate cortex (blue traces). (*E*) Cross-correlation between the tv-fMRI-bs and the 2- to 3-Hz power fluctuations. (*F*) Schematic summarizing the relationships between the 2- to 3-Hz calcium signal, pupil-size changes, and tv-fMRI-bs. (*G* and *H*) Cross-correlation between the pupil size and the calcium signal (2- to 3-Hz power) from the cingulate cortex (*G*) or the barrel cortex (*H*). (*C*, *E*, *G*, and *H*, *Left*) Red dots identify the maximum correlation value from each trial within a ±30-s lag. (*C*, *E*, *G*, and *H*, *Right*) Graphs represent the average ± SD. In the cross-correlation graphs, the lag, indicated in seconds, refers to the variable indicated in the second position of the title (underlined with a horizontal arrow).

analysis of the whole-brain fMRI with pupil dilation, in particular the first derivative of pupil size, demonstrated global negative correlation throughout the brain but specific positive correlation with an area overlapping with noradrenergic cell group A5 located in the brainstem. This ventral pontine activation during pupil dilation was more salient in specific brain states showing uncoupled 2- to 3-Hz and baseline calcium dynamics than in brain states with cross-frequency coupling. In summary, we identified the time-varying fMRI-inferred brain states with concurrent neuronal calcium dynamics, providing distinct correlation patterns to the pupil dynamics in the anesthetized rat brain. Our results suggest that the pupil dynamics observed during anesthesia in rats are directly linked to the global fMRI signal fluctuation (21, 23, 24, 56), as well as to the cortical population activity observed as neuronal calcium transient oscillations, in particular, the 2-3-Ca (Fig. 2, *Bottom* graph, Fig. 4 *G* and *H*, and *SI Appendix*, Fig. S8) (34). A relationship between pupil size and cortical activity, presumably linked to arousal, has been reliably observed in mice during wakefulness and during non-REM (rapid eye movement) sleep (34, 41, 44). These animals also transited between periods of high-amplitude and low-frequency neuronal firing coupled to constricted pupils and periods of low-population activity (i.e., more desynchronized states) linked to pupil dilations, in agreement with our observations. Also, the switch from desynchronized (low-amplitude fast activity) to synchronized (high-amplitude slow waves) EEG in rats anesthetized with isoflurane (57) or urethane (58) has been previously associated with the transition from pupil dilation to constriction, and vice versa (43).

We report 2 findings based on the pupil dynamics–fMRI correlation analysis. One is the global negative fMRI signal related to the pupil dilations (Fig. 3). The observation of cortical regions anticorrelated with the pupil dynamics is in agreement with the arousal-based rs-fMRI signal correlation patterns obtained from unanesthetized nonhuman primates with eye-opening/closing tracking (1). The reduced global BOLD signal observed during pupil dilations in our anesthetized animals coincided with suppressed calcium transient activity from the cortex (2- to 3-Hz calcium fluctuations; Fig. 4*D*), which is in agreement with previous reports of lightly anesthetized rats (21). However, in contrast to the previously reported anticorrelation between cortical and subcortical functional dynamics during vigilant brain states (1, 59–62), the pupil-based fMRI correlation maps in our study showed a rather global negative correlation feature spread over both cortical and subcortical regions (Fig. 3), including the thalamus, which has been reported to be anticorrelated with the cortex in rs-fMRI studies at varied arousal states (63, 64). Wang et al. (4) observed a positive BOLD response in the midline thalamic nuclei coupled to specific astrocytic calcium transients preceding a massive global decrease of the BOLD signal in anesthetized rats. The lack of detection of this fast-positive thalamic BOLD signal from the pupil-based fMRI correlation map may be caused by the largely varied indices of pupil unrest across the different trials (*SI Appendix*, Fig. S5). In addition, the massive global negative BOLD signal may overshadow the phasic positive contribution from the thalamus. A future study integrating concurrent astrocytic calcium signal recording into the multimodal fMRI platform will attempt to further investigate the anticorrelation features of the cortex and thalamus relevant to the brain state.

The second finding is the robust positive correlation observed in a location compatible with noradrenergic cell group A5 from the 1d-pupil–fMRI correlation map (Fig. 3*D*). The neurons of this ventral pontine nucleus send projections to several midbrain areas involved in arousal and vital functions, including the periaqueductal gray and the parabrachial nucleus (50, 65), and are suppressed during REM-like states induced by the acetylcholine agonist

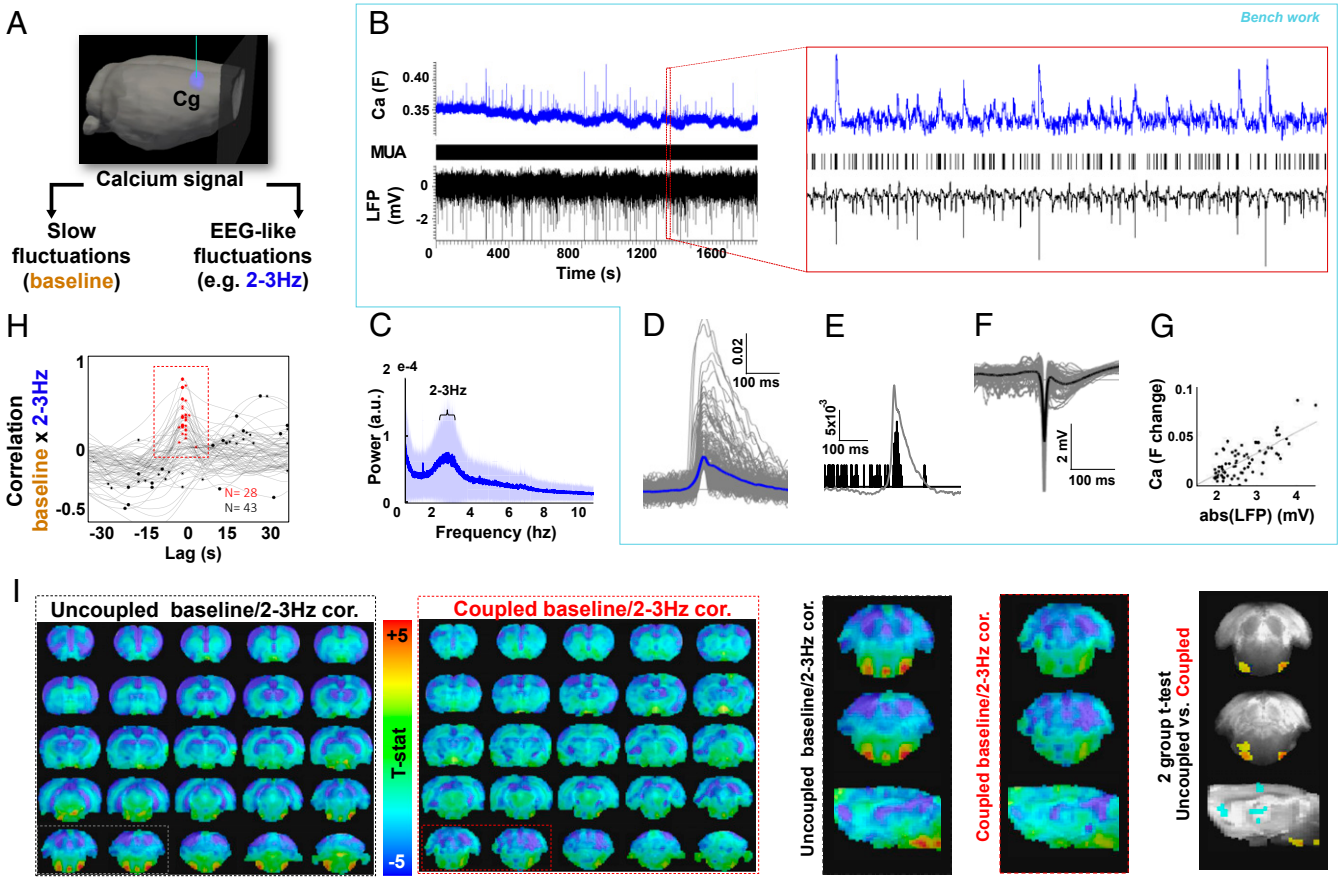


**Fig. 5.** Calcium coupling-dependent cortical states and associated pupil–fMRI patterns. (*A*) The calcium signal can be decomposed into slow (baseline) or relatively fast fluctuations (e.g., 2 to 3 Hz). (*B*) Magnified in a red rectangle are 25 s extracted from a 30-min recording of a GCaMP-based calcium fluorescent signal (in blue) and local field potentials (LFP; in black) recorded simultaneously in a representative animal in the absence of stimulation. (*C*) Power spectrum of the calcium signals of animals undergoing fMRI (average of 64 trials ±SD). (*D*) Average calcium peak. (*E*) Average multiunit activity (MUA) during calcium spikes (the gray curve represents the average calcium spike, for comparison). (*F*) Average LFP peak. (*G*) Correlation between LFP and calcium spikes. (*H*) Cross-correlation between the 2- to 3-Hz band and the baseline (red/black dots: coupled/uncoupled trials). (*I*, *Left*) Maps showing the voxel-wise *t* statistic for a 1-sample *t* test run on the 1d-pupil–fMRI correlation map, for trials with uncoupled (left map) or coupled (right map) calcium signals. (*I*, *Right*) Two coronal slices covering the brainstem and 1 sagittal slice are magnified from both maps to show the differences in A5 correlation values between both groups. The third vertical panel shows the results of a *t* test between both groups (note the significant differences encountered in the A5 area). Maps are thresholded at $P < 0.05$ (FDR correction of 0.99).

carbachol and the alpha-2 receptor clonidine (66), which supports its potential role related to arousal-state fluctuation and pupil-size regulation. Similar to the LC, the A5 noradrenergic area may play an alternative regulatory role in arousal, as suggested from the multiple studies associating noradrenaline with brain-state modulation (67–69). Although brain-state fluctuation and pupil dynamics have been reported to be regulated through noradrenergic projections from the LC (39, 40), we observed no significant positive correlation patterns in the LC or its projection areas. This fact may indicate that the temporal features of pupil dynamics did not serve as a strong linear regressor to fit the neuronal activity-coupled fMRI signal particular to the LC in the anesthetized brain (70, 71). Importantly, to date, the existence of a causal link between the LC and pupil modulation remains to be clarified (49). Further strategies (e.g., noradrenergic-specific cell targeting) will be needed to confirm and characterize the unexplored relationship between the A5 group and pupil dynamics. Additionally, similar to the specific astrocytic-dependent fMRI activation pattern deciphered in anesthetized rats (4), knowledge about the specific dynamic signaling underlying pupil dilations may be needed to identify functional nuclei that may modulate pupil dynamics with particular firing and neurovascular coupling patterns. Also noteworthy is that the A5 area is mostly positively correlated with the first derivative of the pupil rather than the direct pupil size (Fig. 3*C*), which indicates that brainstem activation is more relevant to the change than to the maintenance of the brain state. Cross-correlation of the fMRI signals with 1d-pupil indicated that brainstem activation occurs earlier than global inhibition (the fMRI signal of the A5 area increases in parallel with pupil dilations; *SI Appendix*, Fig. S6*B*), and suggests that the latter might be triggered by the first one; however, a causal link between A5 activation and global cortical/subcortical suppression should be investigated (e.g., with optogenetic experiments).

The concurrent calcium signal acquired with fMRI represents a key advantage to measuring cross-modal brain dynamics. The GCaMP6f-mediated calcium transients, detected with optical fibers, constitute a reliable indicator of neuronal activity (Fig. 5 *B*, *D*, *E*, and *G*), and their spectrogram presents power fluctuation estimates similar to EEG (4, 21). In the present study, 60% of the trials showed a tight coupling between baseline and 2-3-Ca fluctuations, while in 40% of them the calcium dynamics were dissociated. Interestingly, in those uncoupled trials, the pupil-based fMRI correlations were stronger throughout the brain and there was a higher correlation of the calcium baseline with the tv-fMRI-bs (*SI Appendix*, Fig. S9*D*). We observed different coupling from different trials of the same animal and through several animals, which rules out the influence of the optical fiber tip location on the calcium dynamics (i.e., excludes the possibility

that the calcium baseline is determined by the proximity of the implanted optical fiber to a vessel). Also, the brain state-dependent cross-frequency coupling features cannot be simply caused by the blood effect (i.e., the BOLD signal) on the optical fiber-mediated calcium recording. In particular, the largely varied global fMRI signal fluctuation did not match the specific distribution of the calcium cross-frequency coupling, in contrast to the pupil dynamic changes (*SI Appendix*, Fig. S9*C*). This suggested that calcium (un)coupling is associated with brain-state dynamics and does not merely emerge as a result of physiological noise. Specifically, the increased correlation between baseline calcium fluctuations and the fMRI-inferred brain-state vector may be related to spontaneous astrocytic activity, which is known to mark the transition between brain states (4, 55). A previous study also reported an increase of ultraslow electrophysiological activity in conjunction with suppression of higher-frequency bands during arousal switches in mice (55). Our work, involving trials with diverse brain-state dynamics (*SI Appendix*, Fig. S5), has identified different calcium-related conditions that are in agreement with the findings encountered separately in previous reports (21, 55, 56). It is likely that changes in the calcium coupling indicate a shift in the mode of cortical processing (72); however, the meaning and underlying cause of the coupling-dependent states need to be further investigated. The desynchronization between both calcium bands could be associated with arousal pathways emerging at the ventral pons (likely noradrenergic group A5) that may trigger pupil dilations while enhancing global reduction of population activity (2-3-Ca), mostly in cortical neurons. This global regulatory scheme may be necessary to prevent cortical activation from external sources during internal arousal. The dislocation between 2- to 3-Hz and baseline oscillations may reflect a distinct recruitment of both generators (the ultraslow and the 2-3-Ca oscillator) during the arousal fluctuation; however, the source of those cortical dynamics is not sufficiently understood and, hence, any hypothesis remains speculative. Given that all subjects of our study were anesthetized, the degree to which these brain-state changes can be investigated from the data obtained here is limited. Future studies conducted in awake animals should confirm whether these observations can be extrapolated to more aroused brain states that occur during conscious awareness.

Inferring brain-state changes (e.g., fluctuations in the level of arousal) during anesthesia might seem counterintuitive. Arousal has been defined, electrophysiologically, as a state of depolarized neuronal membranes and desynchronized firing (73, 74), also characterized by wide pupils (33, 75), and it is usually assessed during quiet wakefulness or in the context of behavioral performance. Extremely low and extremely high arousal levels yield poorer task performance compared with middle-arousal states, a phenomenon described as an inverted-U relationship (33, 76, 77). Under anesthesia, the brain state is restricted by a maximum arousal level not compatible with consciousness (presumably on the left side of the inverted U) (78). However, in agreement with several reports (54, 57, 58, 79, 80), the present study demonstrates that this state is not confined to a static condition; in contrast, fluctuations in pupil size, which track arousal during wakefulness, were commonly observed in the anesthetized rats and, to the extent at which we could investigate it, the relationship between pupil size and cortical activity is in agreement with what has been observed during wakefulness (dilation linked to decreased population activity). Still, the term arousal or brain-state oscillations in the context of anesthesia remains controversial. One interpretation of having different arousal states under anesthesia relates to the possibility of being more or less susceptible to reaching wakefulness. For example, it is possible that higher brain states observed during anesthesia would require a lower amount of reversal drug to regain consciousness. This possibility could be tested in animals subjected to variable stimulation of the ventral tegmental area, a procedure which has been shown to lead to emergence from general anesthesia (81). Although the meaning of brain-state oscillations remains debatable, together our results suggest that anesthesia is not an isolated unconscious condition but a dynamic oscillatory brain state that can be traced at different scales.

## Conclusion

Here, we identified a quasiglobal negative fMRI spatial pattern that was correlated with pupil dilation and served as a template to produce a brain-state fMRI index during anesthesia. The neurobiological relevance of the linkage between the time-varying fMRI-inferred brain state and the pupil dynamics was verified with concurrent recording of neuronal calcium oscillations in the cingulate cortex. In addition, cross-correlation analysis of the calcium baseline and the 2- to 3-Hz power fluctuation revealed 2 distinct neurophysiological states based on the cross-frequency (un)coupling conditions of the calcium signals. While the global negative pupil–fMRI correlation was present under both states, a positive correlation of the ventral pons was highly linked with uncoupled neuronal calcium dynamics. Altogether, we demonstrate that the pupil size can be tracked in animals undergoing fMRI, allowing to vinculate whole-brain activation patterns with particular brain state-dependent pupil dynamics.

## Materials and Methods

Ten adult rats were used to acquire parallel pupillometry, cortical calcium recordings, and whole-brain fMRI. The study was performed in accordance with the German Animal Welfare Act (TierSchG) and Animal Welfare Laboratory Animal Ordinance (TierSchVersV). This is in full compliance with the guidelines of the European Union (EU) Directive on the protection of animals used for scientific purposes (2010/63/EU). The study was reviewed by the ethics commission (§15 TierSchG) and approved by the state authority (Regierungspräsidium, Tübingen, Baden-Württemberg, Germany). Analysis of the multimodal data included temporal correlation between the pupil dynamics and the fMRI signals, spatial correlation between each fMRI volume and the pupil–fMRI correlation map, and cross-correlation measures between the whole-brain fMRI, the calcium signal at 2 to 3 Hz or baseline, and the pupil size/pupil dilations. A scheme summarizing the main analysis pipeline can be found in *SI Appendix*, Fig. S3. For details concerning surgical procedures, calcium signal acquisition, fMRI sequence, and pupil measures, see *SI Appendix*.

**ACKNOWLEDGMENTS.** This work emerged as part of a PhD thesis supported by the Max Planck Society and the Graduate Training Centre of Neuroscience in Tuebingen (P. Pais-Roldán, "Multimodal assessment of coma and development of fMRI-based methods to study consciousness in the rat," 2019, http://dx.doi.org/10.15496/publikation-34456). The research benefited from funding from the NIH Brain Initiative grants (RF1NS113278-01 and R01 MH111438-01), an S10 instrument grant (S10 RR023009-01) to the Massachusetts General Hospital/Harvard-MIT Program in Health Sciences and Technology Martinos Center, Deutsche Forschungsgemeinschaft (DFG, Germany Research Foundation) grant (YU 215/3-1), and Bundesministerium fuer bildung und forschung (BMBF, Federal Ministry of Education and Research) grant (01GQ1702). We thank Dr. N. Avdievitch and Ms. H. Schulz for technical support, Mr. H. Huang for initial guidance on computer-based pupil-detection algorithms, Dr. E. Weiler, Ms. M. Pitscheider, and Ms. S. Fischer for animal protocol and maintenance support, and the teams of Mr. J. Boldt and Mr. O. Holder for mechanical and electrical support.

1. C. Chang *et al.*, Tracking brain arousal fluctuations with fMRI. *Proc. Natl. Acad. Sci. U.S.A.* **113**, 4518–4523 (2016).
2. B. O. Watson, Cognitive and physiologic impacts of the infraslow oscillation. *Front. Syst. Neurosci.* **12**, 44 (2018).
3. S. H. Lee, Y. Dan, Neuromodulation of brain states. *Neuron* **76**, 209–222 (2012).
4. M. Wang, Y. He, T. J. Sejnowski, X. Yu, Brain-state dependent astrocytic $Ca^{2+}$ signals are coupled to both positive and negative BOLD-fMRI signals. *Proc. Natl. Acad. Sci. U.S.A.* **115**, E1647–E1656 (2018).
5. D. A. McCormick, Neurotransmitter actions in the thalamus and cerebral cortex and their role in neuromodulation of thalamocortical activity. *Prog. Neurobiol.* **39**, 337–388 (1992).
6. X. Liu *et al.*, Arousal transitions in sleep, wakefulness, and anesthesia are characterized by an orderly sequence of cortical events. *Neuroimage* **116**, 222–231 (2015).
7. J. W. de Gee *et al.*, Dynamic modulation of decision biases by brainstem arousal systems. *eLife* **6**, e23232 (2017).
8. B. Biswal, F. Z. Yetkin, V. M. Haughton, J. S. Hyde, Functional connectivity in the motor cortex of resting human brain using echo-planar MRI. *Magn. Reson. Med.* **34**, 537–541 (1995).

9. E. Jonckers, D. Shah, J. Hamaide, M. Verhoye, A. Van der Linden, The power of using functional fMRI on small rodents to study brain pharmacology and disease. *Front. Pharmacol.* **6**, 231 (2015).
10. M. E. Raichle *et al*., A default mode of brain function. *Proc. Natl. Acad. Sci. U.S.A.* **98**, 676–682 (2001).
11. R. Dacosta-Aguayo *et al*., Prognostic value of changes in resting-state functional connectivity patterns in cognitive recovery after stroke: A 3T fMRI pilot study. *Hum. Brain Mapp.* **35**, 3819–3831 (2014).
12. M. D. Fox, M. Greicius, Clinical applications of resting state functional connectivity. *Front. Syst. Neurosci.* **4**, 19 (2010).
13. V. Kiviniemi *et al*., Functional segmentation of the brain cortex using high model order group PICA. *Hum. Brain Mapp.* **30**, 3865–3886 (2009).
14. J. Cabral, M. L. Kringelbach, G. Deco, Exploring the network dynamics underlying brain activity during rest. *Prog. Neurobiol.* **114**, 102–131 (2014).
15. H. Lu *et al*., Rat brains also have a default mode network. *Proc. Natl. Acad. Sci. U.S.A.* **109**, 3979–3984 (2012).
16. D. Mantini *et al*., Default mode of brain function in monkeys. *J. Neurosci.* **31**, 12954–12962 (2011).
17. J. Paasonen, P. Stenroos, R. A. Salo, V. Kiviniemi, O. Gröhn, Functional connectivity under six anesthesia protocols and the awake condition in rat brain. *Neuroimage* **172**, 9–20 (2018).
18. J. L. Vincent *et al*., Intrinsic functional architecture in the anaesthetized monkey brain. *Nature* **447**, 83–86 (2007).
19. J. M. Stafford *et al*., Large-scale topology and the default mode network in the mouse connectome. *Proc. Natl. Acad. Sci. U.S.A.* **111**, 18745–18750 (2014).
20. O. Akeju, E. N. Brown, Neural oscillations demonstrate that general anesthesia and sedative states are neurophysiologically distinct from sleep. *Curr. Opin. Neurobiol.* **44**, 178–185 (2017).
21. Y. He *et al*., Ultra-slow single-vessel BOLD and CBV-based fMRI spatiotemporal dynamics and their correlation with neuronal intracellular calcium signals. *Neuron* **97**, 925–939.e5 (2018).
22. M. Schwalm *et al*., Cortex-wide BOLD fMRI activity reflects locally-recorded slow oscillation-associated calcium waves. *eLife* **6**, e27602 (2017).
23. J. Turchi *et al*., The basal forebrain regulates global resting-state fMRI fluctuations. *Neuron* **97**, 940–952.e4 (2018).
24. M. L. Schölvinck, A. Maier, F. Q. Ye, J. H. Duyn, D. A. Leopold, Neural basis of global resting-state fMRI activity. *Proc. Natl. Acad. Sci. U.S.A.* **107**, 10238–10243 (2010).
25. P. R. Murphy, J. Vandekerckhove, S. Nieuwenhuis, Pupil-linked arousal determines variability in perceptual decision making. *PLoS Comput. Biol.* **10**, e1003854 (2014).
26. M. Schneider *et al*., Spontaneous pupil dilations during the resting state are associated with activation of the salience network. *Neuroimage* **139**, 189–201 (2016).
27. D. Yellin, A. Berkovich-Ohana, R. Malach, Coupling between pupil fluctuations and resting-state fMRI uncovers a slow build-up of antagonistic responses in the human cortex. *Neuroimage* **106**, 414–427 (2015).
28. E. A. Ferenczi *et al*., Prefrontal cortical regulation of brainwide circuit dynamics and reward-related behavior. *Science* **351**, aac9698 (2016).
29. P. Stenroos *et al*., Awake rat brain functional magnetic resonance imaging using standard radio frequency coils and a 3D printed restraint kit. *Front. Neurosci.* **12**, 548 (2018).
30. M. Desai *et al*., Mapping brain networks in awake mice using combined optical neural control and fMRI. *J. Neurophysiol.* **105**, 1393–1405 (2011).
31. C. Hoyer, N. Gass, W. Weber-Fahr, A. Sartorius, Advantages and challenges of small animal magnetic resonance imaging as a translational tool. *Neuropsychobiology* **69**, 187–201 (2014).
32. P. Pais-Roldán, B. Biswal, K. Scheffler, X. Yu, Identifying respiration-related aliasing artifacts in the rodent resting-state fMRI. *Front. Neurosci.* **12**, 788 (2018).
33. M. J. McGinley, S. V. David, D. A. McCormick, Cortical membrane potential signature of optimal states for sensory signal detection. *Neuron* **87**, 179–192 (2015).
34. M. J. McGinley *et al*., Waking state: Rapid variations modulate neural and behavioral responses. *Neuron* **87**, 1143–1161 (2015).
35. T. Knapen *et al*., Cognitive and ocular factors jointly determine pupil responses under equiluminance. *PLoS One* **11**, e0155574 (2016).
36. G. Wainstein *et al*., Pupil size tracks attentional performance in attention-deficit/hyperactivity disorder. *Sci. Rep.* **7**, 8228 (2017).
37. L. Leuchs, M. Schneider, M. Czisch, V. I. Spoormaker, Neural correlates of pupil dilation during human fear learning. *Neuroimage* **147**, 186–197 (2017).
38. M. Schneider, L. Leuchs, M. Czisch, P. G. Sämann, V. I. Spoormaker, Disentangling reward anticipation with simultaneous pupillometry/fMRI. *Neuroimage* **178**, 11–22 (2018).
39. S. Joshi, Y. Li, R. M. Kalwani, J. I. Gold, Relationships between pupil diameter and neuronal activity in the locus coeruleus, colliculi, and cingulate cortex. *Neuron* **89**, 221–234 (2016).
40. P. R. Murphy, R. G. O'Connell, M. O'Sullivan, I. H. Robertson, J. H. Balsters, Pupil diameter covaries with BOLD activity in human locus coeruleus. *Hum. Brain Mapp.* **35**, 4140–4154 (2014).
41. J. Reimer *et al*., Pupil fluctuations track fast switching of cortical states during quiet wakefulness. *Neuron* **84**, 355–362 (2014).
42. J. Reimer *et al*., Pupil fluctuations track rapid changes in adrenergic and cholinergic activity in cortex. *Nat. Commun.* **7**, 13289 (2016).
43. J. E. Kum, H. B. Han, J. H. Choi, Pupil size in relation to cortical states during isoflurane anesthesia. *Exp. Neurobiol.* **25**, 86–92 (2016).
44. O. Yuzgec *et al*., Pupil size coupling to cortical states protects the stability of deep sleep via parasympathetic modulation. *Curr. Biol.* **28**, 392–400.e3 (2018).
45. P. Pais-Roldán *et al*., Raw data for "Indexing brain state-dependent pupil dynamics with simultaneous fMRI and optical fiber calcium recording." Zenodo. https://zenodo.org/record/3677525#.XlBOcPQo-pp. Deposited 21 February 2020.
46. H. Lüdtke, B. Wilhelm, M. Adler, F. Schaeffel, H. Wilhelm, Mathematical procedures in data recording and processing of pupillary fatigue waves. *Vision Res.* **38**, 2889–2896 (1998).
47. R. B. Ebitz, M. L. Platt, Neuronal activity in primate dorsal anterior cingulate cortex signals task conflict and predicts adjustments in pupil-linked arousal. *Neuron* **85**, 628–640 (2015).
48. C. A. Wang, S. E. Boehnke, B. J. White, D. P. Munoz, Microstimulation of the monkey superior colliculus induces pupil dilation without evoking saccades. *J. Neurosci.* **32**, 3629–3636 (2012).
49. V. D. Costa, P. H. Rudebeck, More than meets the eye: The relationship between pupil size and locus coeruleus activity. *Neuron* **89**, 8–10 (2016).
50. C. E. Byrum, P. G. Guyenet, Afferent and efferent connections of the A5 noradrenergic cell group in the rat. *J. Comp. Neurol.* **261**, 529–542 (1987).
51. J. L. Baker *et al*., Robust modulation of arousal regulation, performance, and frontostriatal activity through central thalamic deep brain stimulation in healthy nonhuman primates. *J. Neurophysiol.* **116**, 2383–2404 (2016).
52. G. J. Thompson *et al*., Phase-amplitude coupling and infraslow (<1 Hz) frequencies in the rat brain: Relationship to resting state fMRI. *Front. Integr. Neurosci.* **8**, 41 (2014).
53. M. Siems, M. Siegel, Dissociated cortical phase- and amplitude-coupling patterns in the human brain. bioRxiv:10.1101/485599 (13 June 2019).
54. P. L. Purdon, A. Sampson, K. J. Pavone, E. N. Brown, Clinical electroencephalography for anesthesiologists: Part I: Background and basic signatures. *Anesthesiology* **123**, 937–960 (2015).
55. K. E. Poskanzer, R. Yuste, Astrocytes regulate cortical state switching in vivo. *Proc. Natl. Acad. Sci. U.S.A.* **113**, E2675–E2684 (2016).
56. Y. Ma *et al*., Resting-state hemodynamics are spatiotemporally coupled to synchronized and symmetric neural activity in excitatory neurons. *Proc. Natl. Acad. Sci. U.S.A.* **113**, E8463–E8471 (2016).
57. H. Takahashi, H. Tokushige, T. I. Shiramatsu, T. Noda, R. Kanzaki, Covariation of pupillary and auditory cortical activity in rats under isoflurane anesthesia. *Neuroscience* **300**, 29–38 (2015).
58. T. Blasiak, A. Zawadzki, M. H. Lewandowski, Infra-slow oscillation (ISO) of the pupil size of urethane-anaesthetised rats. *PLoS One* **8**, e62430 (2013).
59. B. Feige *et al*., Cortical and subcortical correlates of electroencephalographic alpha rhythm modulation. *J. Neurophysiol.* **93**, 2864–2872 (2005).
60. G. R. Poudel, C. R. Innes, P. J. Bones, R. Watts, R. D. Jones, Losing the struggle to stay awake: Divergent thalamic and cortical activity during microsleeps. *Hum. Brain Mapp.* **35**, 257–269 (2014).
61. R. I. Goldman, J. M. Stern, J. Engel, Jr, M. S. Cohen, Simultaneous EEG and fMRI of the alpha rhythm. *Neuroreport* **13**, 2487–2492 (2002).
62. Z. Liu *et al*., Finding thalamic BOLD correlates to posterior alpha EEG. *Neuroimage* **63**, 1060–1069 (2012).
63. W. D. Killgore *et al*., Daytime sleepiness is associated with altered resting thalamocortical connectivity. *Neuroreport* **26**, 779–784 (2015).
64. Q. Zou *et al*., Functional connectivity between the thalamus and visual cortex under eyes closed and eyes open conditions: A resting-state fMRI study. *Hum. Brain Mapp.* **30**, 3066–3078 (2009).
65. E. Bruinstroop *et al*., Spinal projections of the A5, A6 (locus coeruleus), and A7 noradrenergic cell groups in rats. *J. Comp. Neurol.* **520**, 1985–2001 (2012).
66. V. Fenik *et al*., A5 cells are silenced when REM sleep-like signs are elicited by pontine carbachol. *J. Appl. Physiol. (1985)* **93**, 1448–1456 (2002).
67. F. Ding *et al*., $\alpha$1-adrenergic receptors mediate coordinated $Ca^{2+}$ signaling of cortical astrocytes in awake, behaving mice. *Cell Calcium* **54**, 387–394 (2013).
68. M. Paukert *et al*., Norepinephrine controls astroglial responsiveness to local circuit activity. *Neuron* **82**, 1263–1270 (2014).
69. J. D. Kenny, N. E. Taylor, E. N. Brown, K. Solt, Dextroamphetamine (but not atomoxetine) induces reanimation from general anesthesia: Implications for the roles of dopamine and norepinephrine in active emergence. *PLoS One* **10**, e0131914 (2015).
70. A. H. Song *et al*., Pharmacological modulation of noradrenergic arousal circuitry disrupts functional connectivity of the locus ceruleus in humans. *J. Neurosci.* **37**, 6938–6945 (2017).
71. D. M. Devilbiss, B. D. Waterhouse, Phasic and tonic patterns of locus coeruleus output differentially modulate sensory network function in the awake rat. *J. Neurophysiol.* **105**, 69–87 (2011).
72. J. F. Poulet, C. C. Petersen, Internal brain state regulates membrane potential synchrony in barrel cortex of behaving mice. *Nature* **454**, 881–885 (2008).
73. A. Renart *et al*., The asynchronous state in cortical circuits. *Science* **327**, 587–590 (2010).
74. M. Steriade, I. Timofeev, F. Grenier, Natural waking and sleep states: A view from inside neocortical neurons. *J. Neurophysiol.* **85**, 1969–1985 (2001).
75. M. M. Bradley, L. Miccoli, M. A. Escrig, P. J. Lang, The pupil as a measure of emotional arousal and autonomic activation. *Psychophysiology* **45**, 602–607 (2008).
76. R. L. van den Brink, P. R. Murphy, S. Nieuwenhuis, Pupil diameter tracks lapses of attention. *PLoS One* **11**, e0165274 (2016).
77. B. J. Schriver, S. Bagdasarov, Q. Wang, Pupil-linked arousal modulates behavior in rats performing a whisker deflection direction discrimination task. *J. Neurophysiol.* **120**, 1655–1670 (2018).
78. M. Bola, P. Orlowski, M. Plomecka, A. Marchewka, EEG signal diversity reflects capability for behavioral responsiveness during propofol sedation. bioRxiv:10.1101/444281 (16 October 2018).
79. R. M. Neves, S. van Keulen, M. Yang, N. K. Logothetis, O. Eschenko, Locus coeruleus phasic discharge is essential for stimulus-induced gamma oscillations in the prefrontal cortex. *J. Neurophysiol.* **119**, 904–920 (2018).
80. C. Curto, S. Sakata, S. Marguet, V. Itskov, K. D. Harris, A simple model of cortical dynamics explains variability and state dependence of sensory responses in urethane-anesthetized auditory cortex. *J. Neurosci.* **29**, 10600–10612 (2009).
81. K. Solt *et al*., Electrical stimulation of the ventral tegmental area induces reanimation from general anesthesia. *Anesthesiology* **121**, 311–319 (2014).
82. G. Paxinos, C. Watson, *The Rat Brain in Stereotaxic Coordinates* (Academic, ed. 6, 2007).